

Seismic Frequency Analysis of Mount Tangkuban Parahu Using IoT-Based MPU6050 Sensor System

Abar Almazari¹, Anggi Faradyba¹, Reyhan Nugraha Akbar¹, I Kadek Agus Sara Sawita¹, Maria Evita^{1*}, Mitra Djamal¹

¹Department of Physics, Bandung Institute of Technology, Bandung 40135, Indonesia

(Received: 2025-06-22, Revised: 2025-10-19, Accepted: 2025-10-27)

Abstract

Indonesia is located at the convergence of three major tectonic plates—the Eurasian Plate, the Indo-Australian Plate, and the Pacific Plate—and lies within the Pacific Ring of Fire, making the country highly prone to seismic activity. Thus, seismic activity is one of the physical parameters used to define the status of a volcano. Consequently, the availability of affordable and accessible early earthquake detection systems is crucial to minimizing infrastructure damage and human casualties. One proposed solution involves the use of the MPU6050 sensor, which is capable of detecting ground acceleration. This sensor has been integrated and installed on a mobile robot for volcano monitoring, which was developed in previous research. In this study, the Fast Fourier Transform (FFT) is employed to convert ground acceleration data into ground frequency, which can then be used to assess seismic activity. Additionally, an ESP32 microcontroller is utilized to collect and process sensor data, which is automatically transmitted via a broker, allowing frequency data and seismic status to be visualized on a dashboard. This research aims to compare acceleration data collected in a laboratory setting (ITB campus) and in the field (Mount Tangkuban Parahu), measure ground vibration frequency at Mount Tangkuban Parahu, and determine the seismic activity status based on the ground vibration frequency at Mount Tangkuban Parahu.

Keywords: esp32, fast fourier transform, ground acceleration, microcontroller, mpu6050, sensor

INTRODUCTION

Indonesia is located in the ring of the fire zone, which causes the area to be very vulnerable to earthquakes and mount eruptions [1]. Volcanoes are geological systems characterized, at any magnitude, by the integral relationship between magma, eruptions, and the formation of a volcanic structure [2]. Active volcanoes are yet another neotectonic expression of plate tectonics [3]. Active volcanoes are dynamic systems that can be instructively compared to active fault zones [4]. Both are subject to stress and strain, both produce distinctive patterns of seismicity and, in a sense, both exhibit stick-slip behavior with similar power-law magnitude–frequency relations [4]. One of the physical phenomena that

can be sensed as a sign of a volcanic eruption is an earthquake. The status of a volcano can be classified based on the measurement of the frequency and magnitude of volcanic earthquakes.

South East Asia and the western Pacific region including Indonesia, is also located at the junction of three major tectonic plates (Pacific plate, Indo-Australian plate, Eurasian plate) [5]. This makes Indonesia highly susceptible to natural disasters, particularly earthquakes of both tectonic and volcanic origin. Earthquakes occur almost daily across the country, ranging from minor tremors to major seismic events. Large-scale earthquakes can cause significant damage to infrastructure as well as considerable

_

^{1*} Corresponding author.

loss of human resources. To mitigate such impacts, early earthquake detection is essential. However, conventional detection instruments such as seismographs are often expensive and inaccessible to the general public. Therefore, one potential solution is the use of the MPU6050 sensor in combination with an ESP32 microcontroller as a cost-effective alternative for early earthquake detection.

There are several calculations related to earthquake scales, such as the Richter scale or Peak Ground Acceleration (PGA), that can be used [6]. The magnitude of an earthquake is measured by the acceleration of bedrock caused by the seismic event [6]. In previous studies [7, 8, 9], the MPU6050 sensor and the Fast Fourier Transform (FFT) method have not been utilized. This absence is mainly due to the sensor's lowcost nature and its limited precision compared to dedicated seismometers, which previously made it less favorable for seismic applications. However, this research highlights the novelty of employing the MPU6050 and FFT demonstrating that, through proper processing and calibration, they can provide a low-cost yet quite effective approach for detecting ground vibration frequency and classifying earthquake status. The sensor system is further enhanced to display both the its corresponding earthquake status and dominant frequency on a dashboard. The detected earthquake frequencies are obtained through the application of FFT. Nevertheless, the frequency and seismic status data cannot yet be displayed in real time, as additional processing is required to convert recorded accelerometer data into corresponding frequency and ground magnitude values.

In this study, the MPU6050 sensor is integrated with an ESP32 microcontroller, which is responsible for collecting and processing data from the sensor. The data is then transmitted via Node-RED, **MOTT** broker to subsequently forwarded to InfluxDB. A portion of the data stored in InfluxDB is directed to a Grafana dashboard, where it is visualized as raw ground acceleration data. This sensor was then placed and integrated with other sensors into a mobile robot. The remaining data is sent to MATLAB, where it undergoes Fast Fourier Transform (FFT) processing to extract the

vibration frequency, magnitude, and determine the seismic activity status. Frequency data collection was conducted in two locations: Institut Teknologi Bandung and Mount Tangkuban Parahu.

The data collection was conducted at the summit of Mount Tangkuban Perahu without internet access. A local WiFi network (without internet) was used to transmit data from the ESP32 to a laptop. Although suitable for laboratory-scale tests, its short range limits field applications in remote or emergency conditions. Therefore, alternative communication methods such as LoRa (Long Range) technology are needed. LoRa uses low-power radio signals to enable long-distance data transmission with minimal energy consumption, typically involving at least two modules—one as a transmitter at the sensor node and another as a receiver at the base station.

METHOD

Seismic Activity

Earthquakes represent the sudden release of slowly accumulated strain energy and hence provide direct evidence of the ongoing tectonic processes. Earthquakes are the result of displacement at depth along faults [10]. A volcanic earthquake refers to an earthquake triggered by a volcanic eruption, characterized by small size and swarm activity [11]. It can be classified into two types: volcanic tectonic earthquakes, caused by the injection or withdrawal of magma beneath the volcano, and long-period earthquakes, resulting from the injection of magma into the surrounding rocks [11].

MPU6050 Sensor

MPU6050 is the 6 degrees of freedom (DOF) sensor that contains 3 axes accelerometer and 3 axes gyroscope [12]. After integrating MPU6050 with Arduino, it produced 3 values that are three axes accelerometer values and 3 axes gyroscope [12]. The MPU6050 sensor is equipped with three 16-bit ADCs (Analog-to-Digital Converters) for converting gyroscope outputs, and three additional 16-bit ADCs for converting accelerometer outputs [13].

NodeMCU ESP32

ESP32 is one of the microcontroller families introduced and developed by Espressif Systems. ESP32 is the successor to the ESP8266 microcontroller [14]. This microcontroller is compatible with Arduino microcontroller already has a WiFi module and is connected to BLE (Bluetooth Low Energy) via a chip, so it is very powerful and can be a good choice for creating an IoT application system [14]. ESP32 stands for Espressif32 which is a development board developed by Espressif Systems [14]. ESP32 is a 32-bit microcontroller equipped with a wireless or wifi network and Bluetooth Low energy (BLE) using the 802.11 b/g/n wifi network protocol that works at a GHz frequency of 2.4 and bluetooth v4.2 technology [14'].

Sensor Characterization

The calibration process of the MPU6050 sensor is illustrated in the following flowchart:

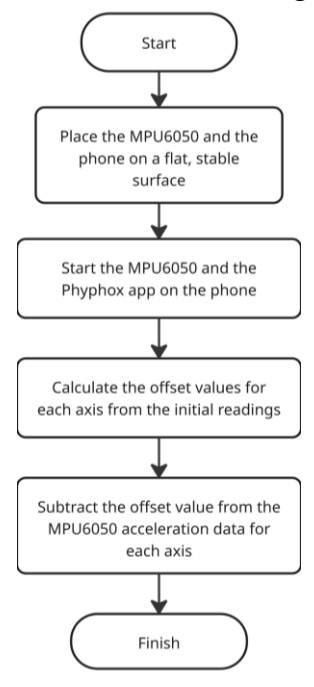


Figure 1. MPU6050 calibration process

Before creating the program needed to further process the sensor data, the first step is to conduct characterization. In this process, we used accuracy characterization. We compared the raw acceleration data from the smartphone's accelerometer using the Phyphox app (Figure 2).

The calibration method we use adopts the principle of comparison calibration, where the

value from the sensor under test is directly compared with a reference standard [15]. In this implementation, the accelerometer sensor on a smartphone, with its data acquired using the Phyphox application, is utilized as the calibrator or reference standard. To ensure both sensors receive identical physical motion input, the sensor to be calibrated (connected to an Arduino) and the smartphone are placed on the same platform, allowing for simultaneous data collection [15].

The difference in values, or offset, between the sensor data and the reference data from Phyphox is then calculated. In the Arduino program, this offset value is used to correct the sensor's output reading in real-time by subtracting it from the raw sensor value. The goal of this process is to minimize the error and ensure that the output of the calibrated sensor more consistent closely becomes and approximates the value indicated by the reference calibrator. This approach represents a practical implementation of end-user calibration that does not require complex laboratory equipment.

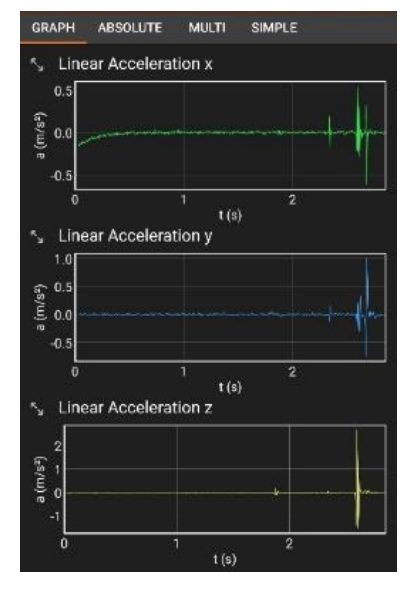


Figure 2. Screenshot of the Phyphox app interface

After aligning the accelerometer axis orientation of the MPU6050 sensor with that of the smartphone sensor, synchronous data acquisition was performed by recording measurements from both devices simultaneously, as show in Figure 3Error! Reference source not found..



Figure 3. Calibration of the MPU6050 sensor with a smartphone sensor as a reference

Before calibration, a comparison graph was obtained between the MPU6050 sensor and the smartphone sensor, as shown in Figure 4.a.

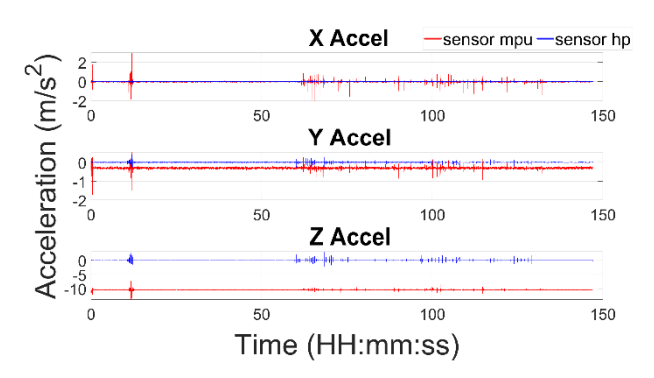


Figure 4.a. Comparison graph of the MPU6050 sensor and the smartphone sensor before calibration

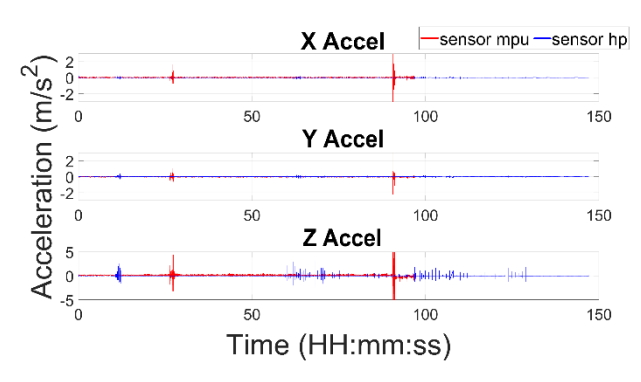


Figure 4.b. Comparison graph of the MPU6050 sensor and the smartphone sensor after calibration

After obtaining the data in Figure 4.a, we added an offset based on the difference between the smartphone sensor data and the MPU6050 sensor data. Then, using the same method as before, we obtained a comparison graph as shown in Figure 4.b.

The calibration and data acquisition process of the MPU6050 sensor is illustrated in the flowchart shown in Figure 4. The system begins by powering on the circuit, after which the device checks for a WiFi connection. If it is not connected, the system continuously attempts to establish the connection until successful. Once connected to WiFi, the device proceeds to connect to the MQTT server (Mosquitto). This step also includes a similar connection check before continuing to the next stage.

After a successful MQTT connection, the MPU6050 sensor begins reading acceleration and angular velocity data. These values are then published periodically to the Mosquitto server.

Next, the data received from the Mosquitto server is separated based on type (acceleration) before being sent to the InfluxDB time-series database. The acceleration data is MATLAB, imported into where signal processing is performed using the Fast Fourier Transform (FFT). The FFT process aims to extract peak frequency values from the recorded vibration data. These peak frequency values are then sent back to InfluxDB and visualized in a dashboard using Grafana. This visualization enables users to monitor vibration data in real time.

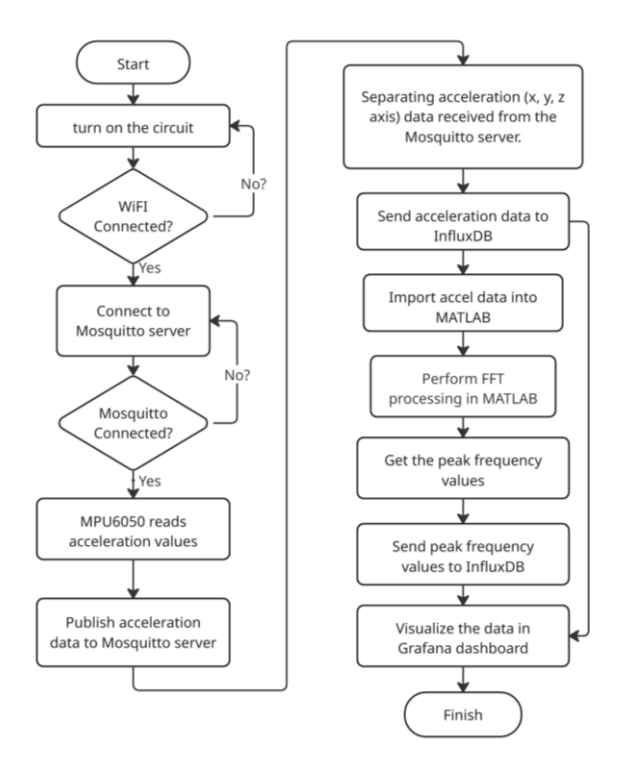


Figure 4. Data processing flowchart

Data Processing Workflow

RESULTS AND DISCUSSION

Environmental Condition

Note that the data from Mount Tangkuban Parahu and ITB were collected on different days, although during similar time intervals. The daytime data were collected between approximately 14:00 and 15:10 UTC+7, while the afternoon data were collected between approximately 15:10 and 16:00 UTC+7. The ITB measurements were conducted specifically in front of the central library building, while the Mount Tangkuban Parahu measurements were taken at a location near the volcano.

Environmental conditions at both sites during data collection were also noted. At the ITB location, the weather was overcast with cloudy skies, and the sensor was placed on a paved surface made of interlocking paving blocks, providing relatively stable ground support. In contrast, the Mount Tangkuban Parahu site experienced clear weather at the beginning of the measurement session around 14:00 UTC+7. A brief light rain occurred at approximately 14:20 and lasted for about five minutes. After the rain, the weather became slightly cloudy. The sensor at this site was placed on a surface composed of small rocks, which have introduced additional micromovements or instability.

Laboratory Testing at ITB

The acceleration data collected at the ITB site, as shown in Figure 5 (daytime) and Figure 6 (afternoon), exhibited relatively stable behavior across all three axes. In Figure 5, the X-axis acceleration ranged from approximately 0.08 to 0.12 m/s², the Y-axis from 0.06 to 0.09 m/s², and the Z-axis from 0.10 to 0.15 m/s². This consistency across time indicates a non-seismic, low-vibration environment typical of an urban setting.

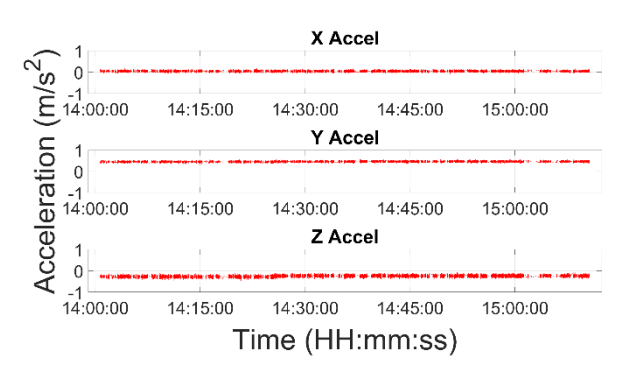


Figure 5. Measurement data collected during the daytime at ITB

A brief data drop-off is visible in Figure 6, likely due to a temporary disconnection of the sensor. This interruption is technical rather than geophysical in nature and does not reflect any change in environmental conditions.

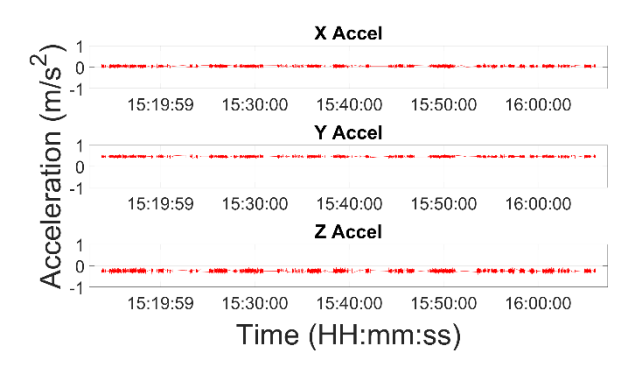


Figure 6. Measurement data collected during afternoon at ITB

The frequency-domain analysis for the testing is shown in Figure 7 (daytime) and Figure 8 (afternoon). Both figures indicate dominant spectral energy below 2 Hz, with a notable peak near 0 Hz. These characteristics are consistent with microtremor activity reported in similar low-seismicity urban environments, particularly within the typical frequency range of 0.8 to 3.65 Hz, as found in a previous study conducted in the Sidoarjo district [16].

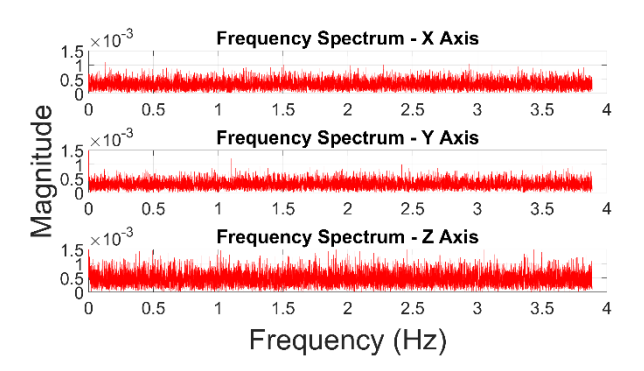


Figure 7. FFT plot from data collected during daytime at ITB

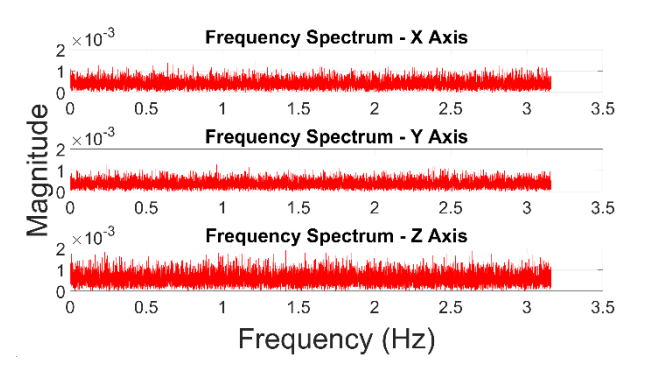


Figure 8. FFT plot from data collected during afternoon at ITB

Field Testing at Mount Tangkuban Parahu

The data collected from Mount Tangkuban Parahu show greater variability and magnitude, as illustrated in Figure 9 (daytime) and Figure 10 (afternoon). In Figure 9, the X-axis values range from approximately 0.10 to 0.20 m/s². The Y-axis shows more fluctuation, reaching up to 0.35 m/s², and the Z-axis records the highest values, peaking around 0.40 m/s². These amplitudes suggest elevated ambient motion, possibly due to microseismic activity or geological resonance near the volcanic structure.

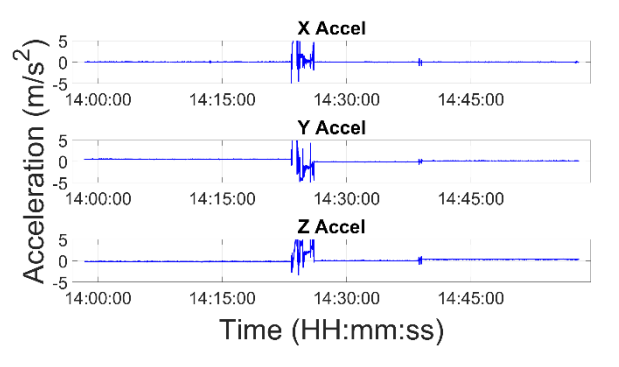


Figure 9. Measurement data collected during daytime at Mount Tangkuban Parahu

In Figure 10, a disturbance is observed around the midpoint of the recording. This corresponds to a brief rain event during which the sensor was repositioned. The resulting fluctuation should be interpreted as environmental noise rather than true seismic signal.

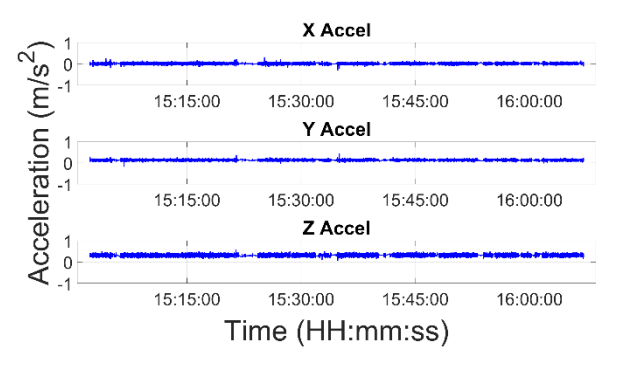


Figure 10. Measurement data collected during afternoon at Mount Tangkuban Parahu

The frequency-domain plots from Mount Tangkuban Parahu (Figure 11 and Figure 12) exhibit dominant spectral peaks in the 1–4 Hz range. This is consistent with previous studies on volcanic microtremor, which typically range from 1–9 Hz, with most energy concentrated between 1–6 Hz as observed at Hakone volcano. These findings confirm that our observations fall well within the expected frequency bands for volcanic seismic activity [17].

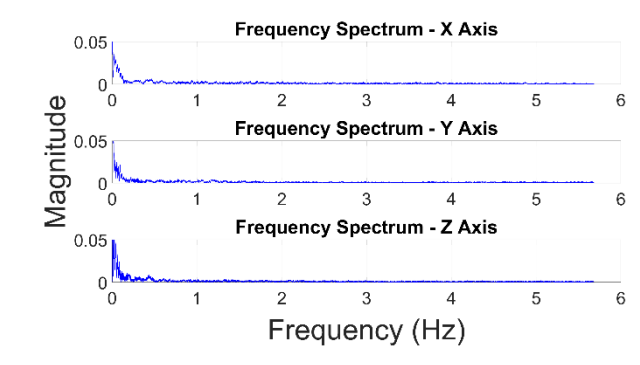


Figure 11. FFT plot from data collected during daytime at Mount Tangkuban Parahu

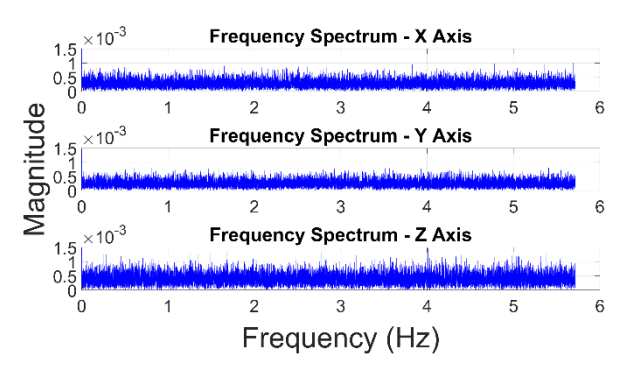


Figure 12. FFT plot from data collected during afternoon at Mount Tangkuban Parahu

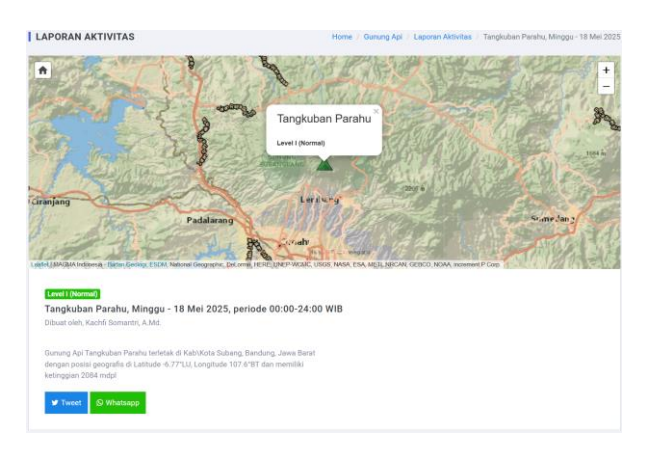
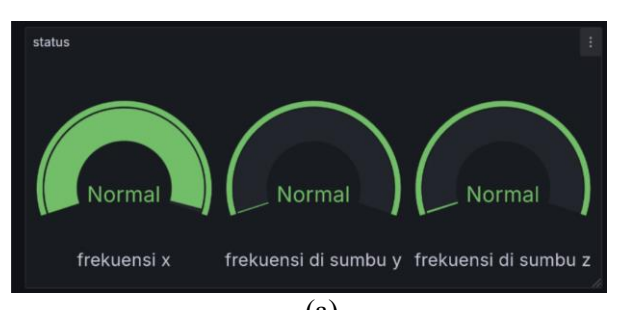


Figure 13. The display of the volcano's condition on the PVMBG website on the data collection date [18].

In general, volcanic tremor has several characteristics, such as an ambiguous onset and unclear phases. The overall frequency range for ground vibration from an active volcano is between 0.5-10 Hz, with a predominant frequency of about 1-3 Hz. The duration of this tremor is also highly variable, ranging from a few tens of seconds, known as isolated tremor, to lasting for ten days or more [19].

According to the official activity report of Tangkuban Perahu Volcano issued by PVMBG on May 18, 2025—the date when our data was collected—the volcano was categorized as Normal by the national vulcanological (Figure 13). This classification aligns with the status displayed on our monitoring dashboard, where key parameters such as seismic frequency (Figure 14), acceleration (Figure 15), readings exhibited stable patterns without detectable anomalies. The consistency between the official field observations and the dashboard visualization demonstrates that the system is

capable of accurately reflecting real-time volcanic conditions.



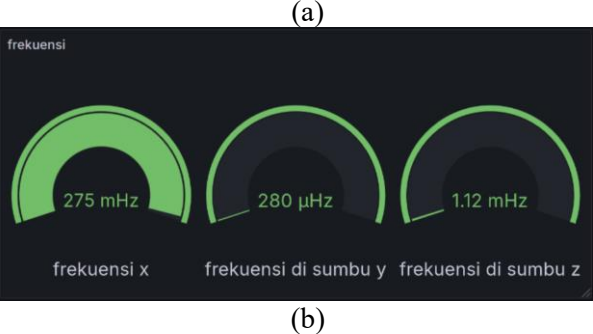


Figure 14. The dashboard displaying the frequency (b) and volcanic status (a) as visualized in Grafana.

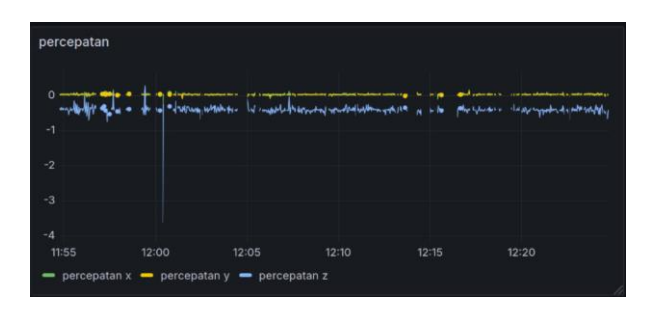


Figure 15. Graph display of acceleration in Grafana.

This agreement highlights the effectiveness of the IoT-based monitoring system developed using open-source tools like Grafana, particularly in its implementation on a volcano seismic monitoring robot. The sensors are optimally integrated into the robotic platform to collect geophysical data accurately and continuously in hazardous and inaccessible areas. By providing intuitive and accessible data visualizations, the system facilitates timely situational awareness and decision-making for both technical personnel and disaster authorities. management Moreover. validation of sensor data against official reports underscores the system's potential in supporting volcanic hazard mitigation through real-time early warning capabilities.

Future development can include the integration of additional sensor modalities, such as volcanic gas emissions, ground deformation (e.g., GPS or tiltmeter data), and surface temperature measurements, to enable a more comprehensive assessment of volcanic activity. System enhancements may also explore the use of machine learning algorithms for automated detection, anomaly thereby improving responsiveness to subtle precursory signals of eruptive activity. With further development and scalability, this framework can be deployed at other active volcanoes across Indonesia—an archipelago with high volcanic risk—and contribute to national disaster risk reduction strategies through robotic and remote monitoring technologies.

CONCLUSION

In conclusion, the system developed using sensor ESP32 MPU6050 and the microcontroller, combined with **MQTT** communication, InfluxDB storage, FFT signal processing in MATLAB, and Grafana visualization, proved effective enough for monitoring ground vibrations in both urban and volcanic environments. The MPU6050 sensor measures acceleration along the X-axis ranging from approximately 0.08 to 0.12 m/s², the Y-axis from 0.06 to 0.09 m/s², and the Z-axis from 0.10 to 0.15 m/s² at the ITB campus. Meanwhile, at Mount Tangkuban Parahu, the X-axis values range between 0.10 and 0.20 m/s². The Y-axis exhibits higher fluctuations, reaching up to 0.35 m/s², while the Z-axis records the highest peaks at approximately 0.40 m/s². The ground vibration frequency ranges obtained from FFT analysis are 275 mHz along the X-axis, 280 microHz (μHz) along the Y-axis, and 1.12 mHz along the Z-axis. These results indicate that the ground vibration frequency remains below the critical threshold of 0.5 Hz, confirming a stable and low-risk volcanic condition based on sensor measurements. This data is visualized in real-time on a Grafana dashboard, which classifies the volcanic activity as "safe" under current monitoring conditions. This indicates that the system is not only capable capturing relevant ground of motion characteristics but also holds potential as a

reliable and low-cost tool for real-time volcanic activity monitoring.

SUGGESTION

For future development, it would be beneficial to use two different types of sensors for comparison. This would help in identifying the most effective sensor option for this application.

ACKNOWLEDGMENT

This study was funded by Institute Technology Bandung through PPMI research grant and the authors are grateful to PVMBG for the permission to do the research at the Mount Tangkuban Parahu.

REFERENCES

- [1] F. Ramdani, P. Setiani, and D. A. Setiawati, "Analysis of sequence earthquake of Lombok Island, Indonesia," Prog. Disaster Sci., vol. 4, p. 100046, 2019, doi: 10.1016/j.pdisas.2019.100046.
- [2] A. Borgia, "What is a Volcano?," *The Geological Society of America Special Paper 470*, 2010.
- [3] A. W. Bally, D. G. Roberts, D. Sawyer, dan A. Sinkewich, "Tectonic and basin maps of the world," dalam Regional Geology and Tectonics (Second Edition), Volume 1: Principles of Geologic Analysis, 2nd ed., Elsevier, 2020, ch. 27, pp. 761–862, doi: 10.1016/B978-0-444-64134-2.00026-2.
- [4] C. G. Newhall, "Volcanology 101 for Seismologists," dalam Treatise on Geophysics, vol. 4, Elsevier, 2007, pp. 351–388, doi: 10.1016/B978-044452748-6.00072-9.
- [5] C. Haberland, M. Bohm, and G. Asch, "Accretionary nature of the crust of Central and East Java (Indonesia) revealed by local earthquake travel-time tomography," J. Asian Earth Sci., vol. 96, pp. 287–295, 2014, doi: 10.1016/j.jseaes.2014.09.019.
- [6] Yulkifli, A. Nofriandi, R. Triyono, W. Audia, and N. A. Sati'at, "Initial Design of IoT-Based Earthquake Intensitymeter Using MMI Scale with Smartphone Display," J.

- Phys.: Conf. Ser., vol. 2734, no. 1, p. 012025, 2024, doi: 10.1088/1742-6596/2734/1/012025.
- [7] M. Evita, A. Zakiyyatuddin, S. Seno, R. Kumalasari, H. Lukado, and M. Djamal, "Development of a robust mobile robot for volcano monitoring application," *Journal of Physics: Conference Series*, vol. 1572, no. 1, p. 012016, 2020. doi: 10.1088/1742-6596/1572/1/012016.
- [8] M. Evita, M. Djamal, B. Zimanowski, dan K. Schilling, "Mobile Monitoring System for Indonesian Volcano," dalam Proc. of 2015 Int. Conf. on Instrumentation, Communications, Information Technology, and Biomedical Engineering (ICICI-BME), Bandung, Indonesia, Nov. 2015, pp. 278–281, doi: 10.1109/ICICI-BME.2015.7401350.
- [9] V. F. Amaliya, H. Lakudo, A. H. Ulum, L. Destarina, S. Seno, F. A. Rakhmadi, N. S. Aminah, M. Evita, and M. Djamal, "Development of IoT-Based Volcano Early Warning System," J. Phys.: Conf. Ser., vol. 1772, p. 012009, 2021, doi: 10.1088/1742-6596/1772/1/012009.
- [10] R. Caputo and S. B. Pavlides, "Earthquake geology: Methods and applications," Tectonophysics, vol. 453, no. 1–4, pp. 1–6, 2008, doi: 10.1016/j.tecto.2008.01.007.
- [11] N. Kumar, D. Hazarika, and K. Sain, "Earthquakes: Basics of seismology and computational techniques," in Basics of Computational Geophysics, 1st ed., Elsevier, 2021, pp. 47–80, doi: 10.1016/B978-0-12-820513-6.00023-0.
- [12] M. M. Afsar, S. Saqib, Y. Y. Ghadi, S. A. Alsuhibany, A. Jalal, and J. Park, "Body Worn Sensors for Health Gaming and e-Learning in Virtual Reality," Computers, Materials & Continua, vol. 73, no. 3, pp. 4763–4777, Jul. 2022, doi: 10.32604/cmc.2022.028618.
- [13] O. O. Artha, B. Rahmadya, and R. E. Putri, "Sistem peringatan dini bencana longsor menggunakan sensor accelerometer dan sensor kelembaban tanah berbasis

- Android," J. Inf. Technol. Comput. Eng. (JITCE), vol. 2, no. 2, pp. 64–70, 2018, doi: 10.25077/jitce.2.02.64-70.2018.
- [14] E. W. Pratama and A. Kiswantono, "Electrical analysis using ESP-32 module in realtime," J. Electr. Eng. Comput. Sci., vol. 7, no. 2, pp. 1273–1284, Dec. 2022, doi: 10.54732/jeecs.v7i2.21.
- [15] A. Umeda, M. Onoe, K. Sakata, T. Fukushi, K. Kanari, H. Iioka, and T. Kobayashi, "Calibration of three-axis accelerometers using a three-dimensional vibration generator and three laser interferometers," Sensors and Actuators A: Physical, vol. 114, pp. 93-101, 2004.
- [16] A. Widodo, J. P. G. N. Rochman, A. Perdana, and F. Syaifuddin, "Seismic Site Effect Mapping Based on Natural Frequency Using Microtremor Method in Sidoarjo District," *IOP Conf. Ser.: Earth Environ. Sci.*, vol. 506, no. 1, p. 012053, 2020, doi: 10.1088/1755-1315/506/1/012053.
- [17] Y. Yukutake, R. Honda, M. Harada, R. Doke, T. Saito, T. Ueno, S. Sakai, and Y. Morita, "Analyzing the continuous volcanic tremors detected during the 2015 phreatic eruption of the Hakone volcano," *Earth, Planets and Space*, vol. 69, no. 164, 2017, doi: 10.1186/s40623-017-0751-y.
- [18] K. Somantri, "Laporan Aktivitas Gunung Api Tangkuban Parahu, Minggu 18 Mei 2025, periode 00:00-24:00 WIB," MAGMA Indonesia, 18 Mei 2025. [Daring]. Tersedia: https://magma.esdm.go.id/v1/gunung-api/laporan/285209?signature=737ff3f4ad0 593c9e80447ab5a0f9cac927965773d57f6f 086b69ba8b3d0db15. [Diakses: 20 Juni 2025].
- [19] S. R. McNutt and T. Nishimura, "Volcanic tremor during eruptions: Temporal characteristics, scaling and constraints on conduit size and processes," *J. Volcanol. Geotherm. Res.*, vol. 178, no. 1, pp. 10–18, 2008, doi: 10.1016/j.jvolgeores.2008.03.010.